A Machine Vision System for Stacked Substrates Counting With a Robust Stripe Detection Algorithm

Hong Zhao, Rong Dai, and Changyan Xiao

***Abstract*—Batch measurement of sheet-like product quantity is very common in manufacturing and commercial areas. Particularly, to satisfy the growing requirement of automatic and nondestructive detection, a machine vision system for stacked substrates counting is proposed in this paper. With a brief description of the system architecture and imaging module, the challenges for real data analysis are investigated. Our main contribution is to develop a robust stripe detection algorithm by combining the merits of local template matching and global frequency domain filtering. Besides the peak-valley feature across the stack profile, the collinear prior shape along the substrates is also utilized in a morphological scheme to purify the obtained ridge-line or stripe images, which, finally, benefits the statistical counting output. It is verified in experiments using a diversity of substrate media that our developed system can achieve a high counting accuracy with the detection error not more than 0.01% as the sample thickness varies between 0.05 mm and 0.5 mm. Moreover, the proposed algorithm performs much robustly with various kinds of abnormalities and interferences like irregular piling, media distortion, and foreign contamination.**

***Index Terms*—Comb filter, machine vision, pattern matching, substrate counting.**

I. Introduction

MANY manufacturing and commercial processes like the quality control and product delivering in printing, packaging, banking, mining, and photovoltaic industry [1]–[6] often result in stacks of thin planar substrates such as printed papers, plastic cards, and metal sheets, which need be counted to enable a segregation of a particular quantity for subsequent processing or sale. Particularly, ascertainment of the stacked quantity is more necessary for inventory or cost control purposes [7]. However, counting of stacked substrates might be difficult due to their very thin structure, large batch amount, low contrast for recognition, and complicated interferences in applications.

Manuscript received August 8, 2017; accepted October 12, 2017. Date of publication November 20, 2017; date of current version October 15, 2019. This work was supported by the National Science Foundation of China under Grant 61571184, Grant 61733004, and Grant U1613209. This paper was recommended by Associate Editor M. Celenk. *(Corresponding author: Changyan Xiao.)*

The authors are with the College of Electrical and Information Engineering, Hunan University, Changsha 410208, China (e-mail: hongzhao@hnu.edu.cn; c.xiao@hnu.edu.cn).

Color versions of one or more of the figures in this paper are available online at http://ieeexplore.ieee.org.

Digital Object Identifier 10.1109/TSMC.2017.2766441

The conventional counting approaches typically involve measuring the overall height or weight of the stack, and the quantity is then inferred by dividing by the average parameter [8]. Because the tiny attribution variation of individual substrate could be accumulated and reach a large deviation with a high stack, the accuracy of the inferential methods might appear low in the case. Additionally, as a simulation of manual operation, mechanical rotating discs were developed for sequentially isolating and flipping each substrate in the stack with a pneumatic device [9]. One drawback of such mechanical methods is that the moving and touching parts may damage the substrates being counted, which is strictly prohibited in some areas as high-end printing or fragile articles. Furthermore, the mechanical system often suffers from a comparatively slow speed, and the counting errors frequently arise from insufficient or unsuccessful separation of items within the stack.

Recently, as a noncontact measurement technique, machine vision methods have attracted more attention [10]–[12]. Depending on the imaging sensors, machine vision-based substrate counting systems can be classified into several categories such as laser scanner [13], 1-D linear array camera [14], and 2-D area array camera-based schemes [15]. Among them, the laser scanning scheme is often assisted by a linear motor to reach the whole stack range. The additional mechanical motion makes it unsuitable for high-speed applications. The 1-D linear array camera receives the reflected light from the substrates and inherently generates a signal waveform responsive to surface attribute variations across the stack. The merit of linear camera schemes is to achieve rapid measurement with a comparatively low cost [14], but their obvious drawback is on noise suppression and abnormality adaptation. With a large increase of imaging resolution and computing speed, the area camera schemes are becoming more popular in recent years. With the additional spatial information, the 2-D lateral images from area cameras are expected to provide more accurate measurement if configured with appropriate post-processing algorithms.

Behind the above machine vision schemes, the signal or image processing algorithms play a critical role, which directly determine the counting accuracy. Although the most related work was reported in the form of patent with much interest in system design, there still existed several groups focusing on the post-processing algorithm development. Since the laser scanner and linear CCD camera directly output an 1-D reflection signal of the stack profile, the early studies mainly concerned on detecting the peak pattern corresponding to individual substrate fringe. Bittar and Perdoux [1]

and Auboussier *et al.* [16] utilized the relevant information between the substrate and intersubstrate gap for counting, which can be efficiently implemented but strongly depends on the accuracy of peak finding. Harba *et al.* [17] presented a frequency domain filtering method to locate individual substrates. Their algorithm is based on an assumption that the testing items have equal thickness and gap width, and consequently might fail in case of inhomogeneous stacks. Recently, Chen *et al.* [18] proposed a real-time sheets counting approach, which utilized a bi-Gaussian kernel filter and a ridge-valley descriptor to improve adjacent objects identification. With a wide spreading of area cameras, the 2-D stack image analysis is drawing more effort. For example, Petker *et al.* [2] presented a wavelet-based multiscale filter to enhance the banknote edges. After fusion with the original stacking image, an adaptive threshold algorithm is adopted to binarize the merged image and a counting algorithm simulating the human behavior is specifically applied to obtain the final result. Gang *et al.* [19] implemented a line segment detection algorithm for stacked paper quantity measurement using a gradient guided growing strategy, and their contribution is mainly on the substrate stripe linking. Suppitaksakul and Rattakorn [3] developed a machine vision system to count corrugated cardboards, where the morphology operators were utilized for shape analysis and edge detection. Similar applications can also be referred to automated counting of palletized slate slabs [4], Solar Wafers [5], printed circuit boards [6]. Although plausible results were reported in the previous work, a common problem behind is that the image analysis and counting algorithms appear insufficiently robust especially facing the challenges like sticky and hiding substrate or presence of contaminations on the stack surface.

In this paper, we will present a machine vision system using 2-D area cameras for quantity measurement of stacked substrates. With a concise introduction of system configuration, our emphasis is put on the post-processed image analysis. Motivated by an observation that the substrate fringes appear as approximately equidistant and parallel straight lines in the stack side image, we will present a novel stripe detection algorithm by merging the periodical repetition pattern and prior shape information.

The remainder of this paper is organized as follows. Section II introduces the imaging system and challenges of data analysis. The counting algorithm is described in Section III. Section IV gives the experiment results and the comparison with other methods. Finally, the conclusion is drawn in Section V.

II. System Architecture and Data Property

In this section, we first introduce the architecture and configuration of the counting apparatus as a machine vision system [20], then investigate the challenges for image analysis and substrate detection.

A. System Architecture

The developed apparatus is a typical machine vision system and can be divided into three parts as shown in Fig. 1(a): 1) the chassis and mechanical components; 2) an imaging module; and 3) a processing module. Among them, the chassis and related mechanical components provide a support for stack alignment and imaging components installation, which also protect the interior modules from environmental stains. The imaging module is used for capturing the stack lateral images. The processing module is a microcomputer ① configured with an Intel Celeron CPU and 4 GB RAM.

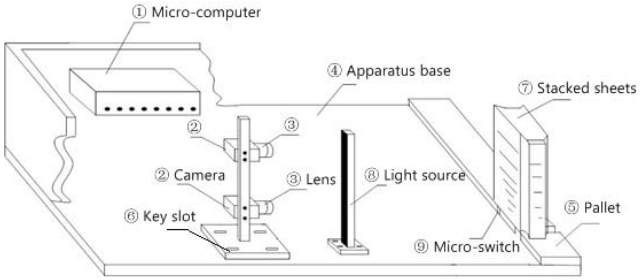

(a)

(b)

Fig. 1. System architecture of the proposed apparatus. (a) Layout of hardware modules. (b) Apparatus photograph.

Furthermore, the core of the imaging module is an industrial camera ②, with a $1/2''$ Rolling Shutter CMOS sensor, providing 2592×1944 active pixels at a maximal frame rate of 8 frames/s. The camera is combined with a 32 mm focal length prime lens ③. Cameras and lens are directly mounted on the shaft which is installed on the apparatus base ④. The working distance between lens and the pallet ⑤ can be adjusted by moving shaft along the key slot ⑥ to measure the stacks ⑦ with different thickness.

As an illumination, a high intensity LED strip ⑧ is fixed to the front side of the pallet to cancel out the influence of ambient light and produce the best image quality in terms of contrast and visibility of a single substrate. The LED shines is controlled and synchronized with the micro switch ⑨ by an internal flash controller.

Fig. 1(b) is a photograph of the developed apparatus. Generally, the measurement procedure is as follows. While the measured stack is loaded on the pallet, the microswitch is triggered to turn on the LED light. After manually aligning the substrate fringes to the panel plane, the flank of the stack is imaged with the cameras and the object remains stationary during the imaging procedure. Then, the cameras deliver the images to the industrial microcomputer for analysis through a universal serial bus interface. The developed counting software installed on the microcomputer is responsible for the image analysis and quantity measurement.

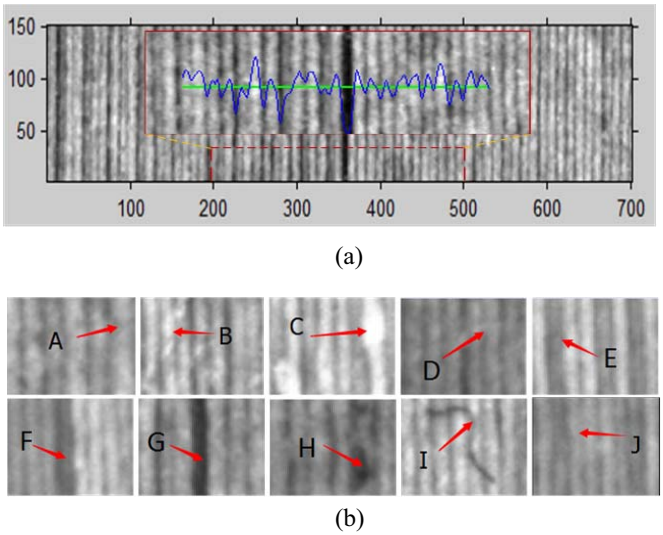

Fig. 2. Demonstration of a stacked substrate image and typical abnormalities. (a) Lateral image from a pile of papers. Here, the red dashed rectangle labeled region is zoomed and overlaid on the original image, the blue curve corresponds to a gray-value profile along the green solid line. (b) Typical local abnormalities as marked with red arrows, i.e., A. irregular deformation, B. burr, C. coarse edge, D. touching or sticky substrate, E. broken fringe, F. hiding substrate, G. broaden gap, H. stained fringe, I. foreign object contamination, and J. low-resolution imaging artifact.

B. Data Property and Challenges

A sample of the 2-D stack side image acquired with the above imaging system is shown in Fig. 2(a). Here, a stack of printed papers with thickness around 0.08 mm is used for demonstration. As observed, the line-shaped stripes corresponding to individual substrates take a global periodical repetition across the stack, but the inhomogeneous gray-value distribution and varying contrast are commonly seen, which is especially obvious with the 1-D profile, see the blue curve. Moreover, many local abnormalities arisen from complex factors like irregular alignments, coarse fringe surfaces, or foreign object contaminants increase the difficulty of image analysis.

To further understand the challenges of substrate identification, we extract subregions containing typical abnormalities from different stack images [see Fig. 2(b)]. According to the generating causes, these abnormalities can be classified into four categories.

1) *Substrate Quality Deterioration [A–E in Fig. 2(b)]:* During manufacture, packaging, and handle processing, the quality of substrates might be accidentally changed with various factors. For example, the irregular deformation (A) often comes from an inhomogeneous bending after a long time of piling up; the burrs (B) along the substrate fringe results from a blunt blade cutting process; a coarse edge (C) is caused by storing in a damn environment or the wear and tear from frequent movement; the touching or sticky substrates (D) are attributed to the presence of improperly cut fibers extending at least in part across neighboring substrates; and the broken fringes (E) often arise from the torn substrates.
2) *Irregular Stack Alignment [F and G in Fig. 2(b)]:* Due to their soft structure, the piling operation of thin substrates like paper might generate a large friction between neighboring substrates, which makes it difficult to keep all the substrate fringes in the same vertical plane during measurement. A hiding substrate (F) is thus caused with a single substrate being trapped inside the stack. Whereas, the broaden gap (G) usually comes from a local bending deformation of the concerned substrate, especially after a long time of preservation.
3) *External Contaminants [H and I in Fig. 2(b)]:* The manufacture, transportation, or even preservation procedures are easy to introduce some external contaminants. For example, the stains fringe (H) is covered by dust or grit, and the foreign object (I) might come from adhering external material fibers.
4) *Imaging Artifacts [J in Fig. 2(b)]:* The gap between adjacent substrates is very narrow especially under external force compressing. Therefore, with an insufficient resolution of lens or camera configuration, the intersubstrate gap will become unrecognizable. This is called a low-resolution imaging artifact (J).

III. Substrate Counting Algorithms

Based on previous analysis, we will present a four-stage algorithm for substrate stripe detection as well as quantity measurement in this section. Generally, our scheme adopts a robust peak detection strategy to locate the substrate fringes across different 1-D profiles, and the detected ridge lines of stripes are purified with a line shape constraint to achieve final counting.

As shown in Fig. 3, the overview pipeline of our proposed algorithm is divided into four steps.

1) *Preprocessing Operation:* For an input 2-D stack side image $I(x, y)$, its profile along the kth row is extracted and denoted as $S_o(x, y_k)$. Then, a comb filter is applied to obtain the preprocessed or filtered signal $F_c(x, y_k)$.
2) *Template Matching and Correlation Measurement:* With the preprocessed profile signal $F_c(x, y_k)$, we can not only locate the potential substrate fringe by finding its peaks but also synthesize an optimal template $T_o(x)$ from the average peak shape. Then, a pattern match is realized by calculating the cross-correlation (CC) $R^*_{\text{ncc}}(x, y_k)$ between $T_o(x)$ and the original signal $S_o(x, y_k)$.
3) *Fusion and Verification:* The comb filtering and template matching methods, respectively, have their specific pros and cons. Their merits are integrated in a complementary and posterior verification way to improve the substrate fringe detection.
4) *Post-Processing and Statistical Counting:* After processing all the rows of $I(x, y)$ with a loop from steps 1–3, a 2-D ridge line image can be generated by combining the detected peak points. To further suppress noise and interference, a prior shape-based morphological operation is applied to purify the stripe lines. And a statistical counting across multiple profiles is adopted to get the final measurement.

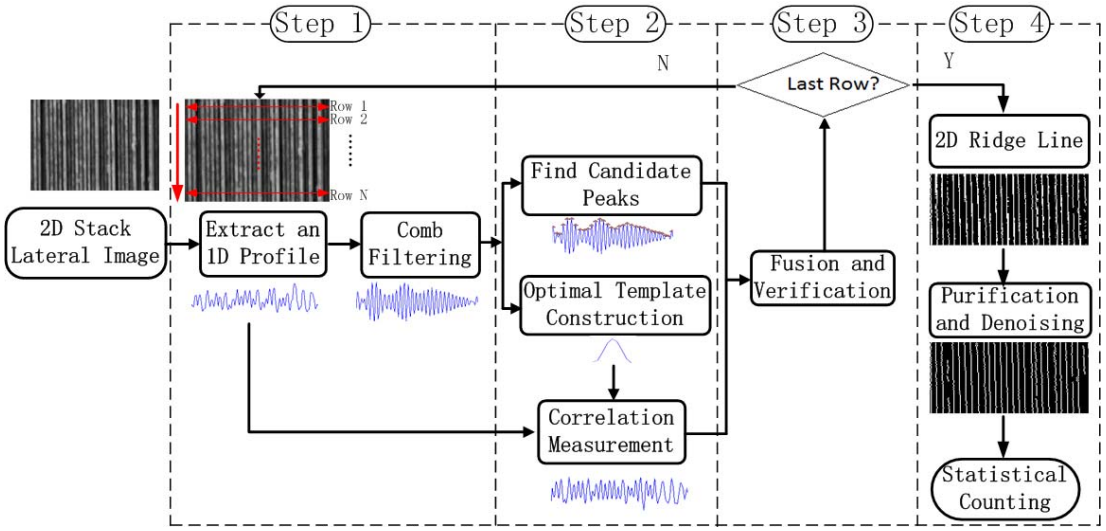

Fig. 3. Pipeline of the proposed counting algorithm. The steps 1–4 correspond to the preprocessing filtering operation, peak detection, template matching and correlation measurement, fusion and verification, and post-processed counting, respectively.

A. Step1: Preprocessing Operation

The purpose of the preprocessing step is to filter out the noise and increase the contrast between the substrates and their interregional gap. Inspired by [17], we introduce a comb filter which only keeps the high-energy harmonic components to separate the quasi-periodic signal from the noise. As shown in Fig. 3, an 1-D profile $S_o(x, y_k)$ is first extracted from the kth row of an input 2-D stack lateral image. For demonstration, we calculate the Fourier transformation (FT) $\widehat{S}_o(n, y_k)$ of the $S_o(x, y_k)$ signal and give its magnitude in Fig. 4(a). As shown, the first magnitude peak denoted as h_0 is called the fundamental (or first harmonic) and the other peaks denoted as h_1 and h_2 are called the harmonics. Because the stack profile has a strong periodic character, the fundamental and harmonics contain the most energy in $S_o(x, y_k)$.

The comb filtering is done by truncating the FT of the 1-D profile signal, i.e., $\widehat{S}_o(n, y_k)$ as illustrated in Fig. 4(a). Only the frequencies around the harmonics are kept, and the frequency band widths are marked with dashed-line rectangles in the spectrum plot. To give a mathematical expression, we have

$$\widehat{F}_c(n, y_k) = \begin{cases} \widehat{S}_o(n, y_k) & \text{if } \min_{i=0,1,2,\ldots}\{\|n - h_i\|\} \le b_p \\ 0 & \text{otherwise} \end{cases} \quad (1)$$

where $\widehat{F}_c(n, y_k)$ denotes the spectrum of filtered signal, h_i represents the $(i+1)$th harmonic location with $p = 2b_p$ being the band width. Thus, the frequencies that are distant from harmonics and may correspond to local deviations among thin substrates are eliminated. In other words, the purified information useful for counting is kept in $\widehat{F}_c(n, y_k)$, whose time domain representation $F_c(x, y_k)$ can be easily obtained with an inverse FT. Note the essence of the comb filter is to match the original signal with a series of periodic harmonics in a global manner. Its outstanding merit is able to explore the implicit quasi-periodic pattern even in a seriously noisy environment.

To demonstrate the effect of comb filtering, we select a segment of stack profile and illustrate it in Fig. 4(b). This profile includes a weak substrate fringe and a widened gap, respectively, labeled with G and H. The comb filtered signal is given in Fig. 4(c). Here, we only preserved the first three fundamental and harmonics. As shown, the periodicity of fringe peaks appears much obvious after filtering, even with the very weak substrate. However, the spectrum filtering is generally a global pattern matching scheme, which lacks the flexibility and adaptability on local abnormalities. Therefore, two false peaks incorrectly occur at the widened gap region to keep the periodical repetition [see Fig. 4(b)-H].

B. Step 2: Template Matching and Correlation Measurement

Different from the spectrum filtering, the template matching depends on a local correlation measurement to determine the presence of an object, where the construction of template plays an important role. First, we select various kinds of normal substrate profiles as candidate templates from the preprocessed signal. For example, as the red rectangles marking regions in Fig. 4(c), only the peaks corresponding to real substrates and their original gray-level above a threshold are selected to define the template. Second, considering the gray-level variance for different candidate profiles, an under curve area normalization is applied to reduce the impact during template synthesis. To give a mathematical presentation, we have

$$T_n(x) = t(x)/A \quad (2)$$

where $t(x)$ denotes a candidate profile with A being its covering area and $T_n(x)$ is the normalized result. Finally, the normalized profiles are aligned at their peak locations and the curves are directly accumulated to calculate the average shape, which is considered to be the optimal template for subsequent work. This can also be formulated as

$$T_o(x) = \sum_{i=0}^{m-1} T_{n_i}(x)/m \quad (3)$$

with m being the number of previously normalized candidate profiles (i.e., T_{n_i}) and T_o being the optimal template.

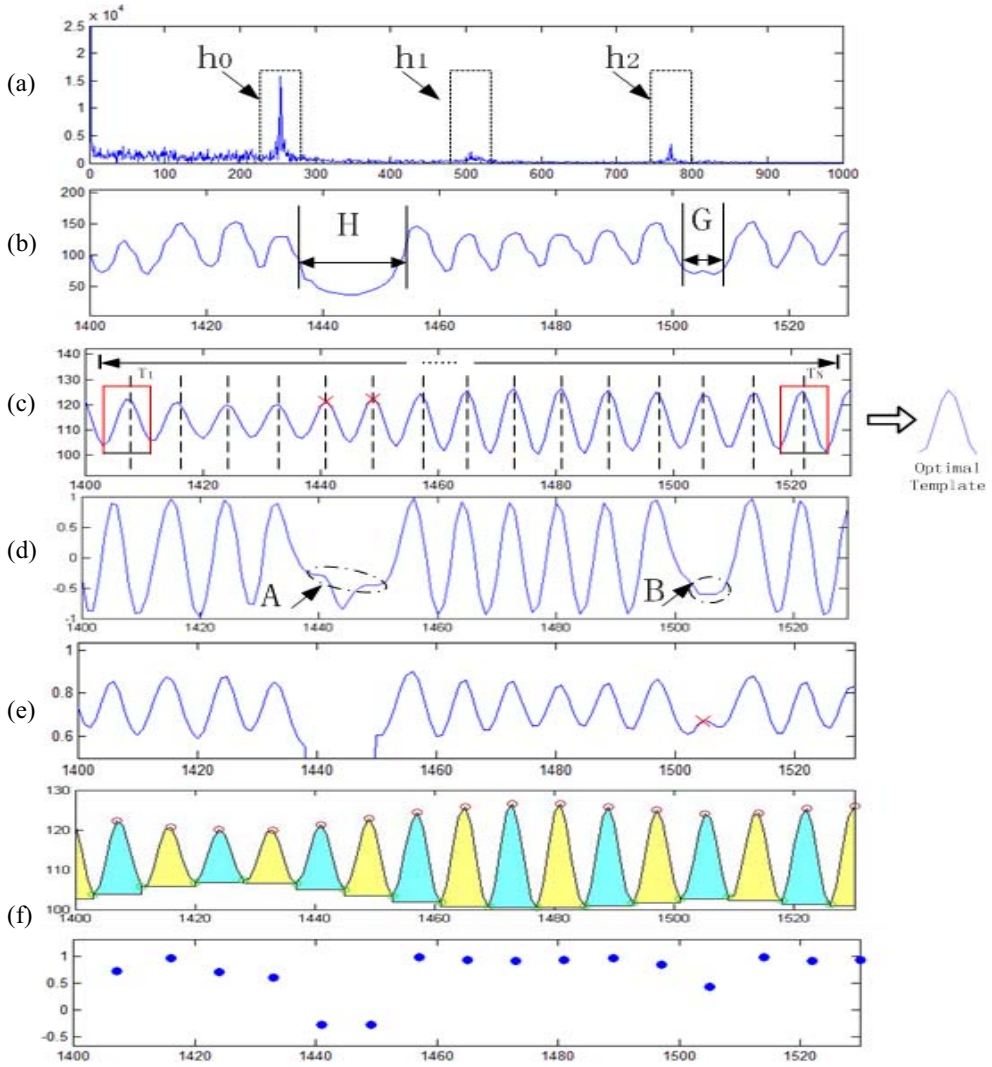

Fig. 4. Detecting along an 1-D profile. (a) Amplitude spectrum of the original signal and the comb filter configuration. (b) Original signal S_o. (c) Comb filtered signal F_c. (d) ZNCC measure R_{zncc}. (e) Improved NCC measure R_{ncc}. (f) Fusion and verification result P_{ncc}.

For clarity, we demonstrate the procedure of optimal template generation using four candidate templates in Fig. 5. Here, the original profiles $t_1 - t_4$ are plotted in Fig. 5(a), and the normalized and aligned profiles are given in Fig. 5(b) with the synthesized template being overlaid in bold red line.

There are several traditional correlation measurements and their variants, which are used for template matching. Among them, the popular CC is a measure of similarity of two series as a function of the displacement of one relative to the other, which usually works to search a long signal for a shorter known pattern or feature. In discrete signal processing, the CC is defined as

$$R_{\text{cc}}(u) = \sum_{i=0}^{m-1} f(u+i)t_o(i) \tag{4}$$

with t_o being the template, f the signal, and m the template length. Note the CC is equivalent in nature to the convolution of two functions if the template signal is symmetrical around the center. To make it brightness and contrast invariant, a normalized CC (NCC) is termed as

$$R_{\text{ncc}}(u) = \frac{\sum_{i=0}^{m-1} f(u+i)t_o(i)}{\{\sum_{i=0}^{m-1} f(u+i)^2 \sum_{i=0}^{m-1} t_o(i)^2\}^{0.5}}. \tag{5}$$

Further, considering the influence of background offset, the zero-mean NCC (ZNCC) was presented to tolerate the uniform brightness variation, which can be reformulate to

$$R_{\text{zncc}}(u) = \frac{\sum_{i=0}^{m-1}\left[f(u+i) - \overline{f_c}\right]\left[t_o(i) - \overline{t_o}\right]}{\left\{\sum_{i=0}^{m-1}\left[f(u+i) - \overline{f_c}\right]^2 \sum_{i=0}^{m-1}\left[t_o(i) - \overline{t_o}\right]^2\right\}^{0.5}} \tag{6}$$

with $\overline{f_c}$ and $\overline{t_o}$ being the mean values of f_c and t_o, respectively.

Although the ZNCC formulation was reported to provide the better robustness in background suppression [21], [22], it is not much suitable for the substrate fringe detection in our work. To explain this, we choose an irregular weak fringe profile corresponding to the G labeled segment in Fig. 4(b) for demonstration. After removing the background offset, the zero-mean signal and template are zoomed and illustrated in

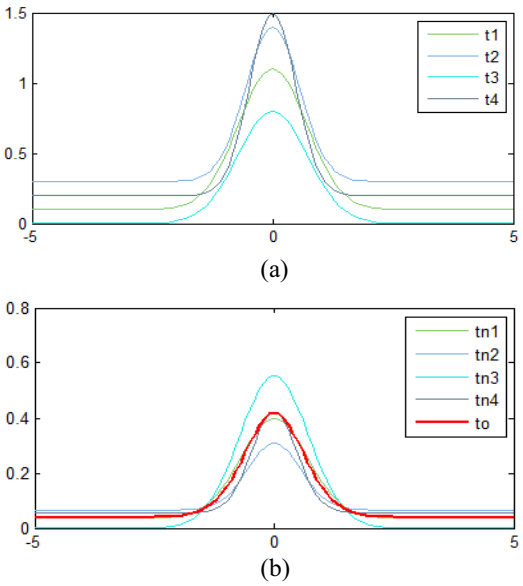

Fig. 5. Synthesize an average or optimal template. (a) Original profiles $t_1 - t_4$. (b) Normalized profiles $tn_1 - tn_4$, which were aligned and averaged to generated the average or optimal template overlaid in a bold red line.

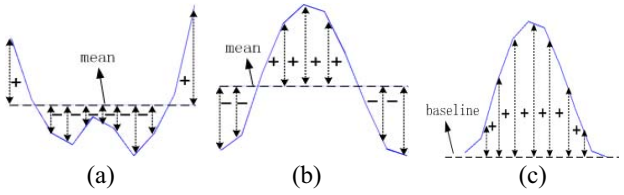

Fig. 6. Investigate the effect of different CC measures on weak signals. Here, (a) indicates a weak substrate profile from the segment G in Fig. 4(b). The equivalent filtering kernels for the ZNCC and our modified NCC are given in (b) and (c), respectively.

Fig. 6(a) and (b), respectively. Here, because the CC is equivalent to a convolution operation and the zero-mean template resembles an inverse second-order Gaussian kernel, the ZNCC will perform like a second-order derivative operator in our work. It essentially calculates a weighted sum between the signal main-lobe and its side-lobes. As shown with Mark B in Fig. 4(d), an unexpectedly negative response was obtained due to the irregular and weak main-lobe in this case. Another problem is with the step edge as marked with A in Fig. 4(d), where the gap slopes are wrongly identified as an object. This is a well-known drawback of the second-order derivative operator especially in the medical blood-vessel image analysis field [23].

Different from the ZNCC measure, the NCC operation essentially conducts a Gaussian-like smoothness, where the convolution kernel is the normalized optimal template. However, the original NCC also performs not well on the weak fringes profiles. As an improvement, we first remove the baseline and normalize the optimal template to a standard smoothing kernel with the area under curve being one. Here, the normalized template is given in Fig. 6(c), which obviously resembles a zero-order Gaussian kernel. Then, a threshold is exerted on the numerator term, which helps to suppress

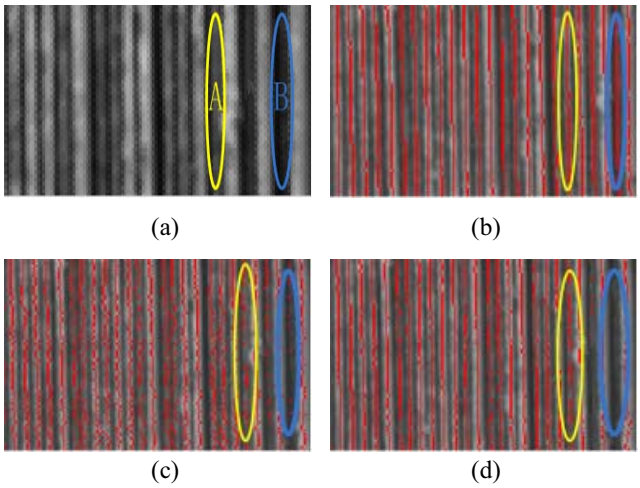

Fig. 7. Illustrate the fusion and verification result. (a) Original 2-D stack lateral image. (b) Ridge lines which are generated from the peaks of the comb filtered signal F_c. (c) Ridge lines obtained from the improved NCC result R^*_{Ncc} by selecting the peaks whose correlation measure value is above 0.8. (d) Fusion and verification result P_{ncc} derived from the (b) and (c) through ZNCC produces the ridge lines.

the false response on the step edges. To give a mathematical presentation, we have

$$R^*_{\text{ncc}}(u) = \frac{W^*(u)}{\left(\sum_{i=0}^{m-1} f(u+i)^2 \sum_{i=0}^{m-1} t_o(i)^2\right)^{0.5}} \tag{7}$$

where

$$W^*(u) = \begin{cases} \sum_{i=0}^{m-1} f(u+i)t^*(i), & \text{if } R_{\text{cc}} > \text{th}_1 \\ 0, & \text{otherwise} \end{cases}$$

and $t^*(i) = (t_o(i) - \min(t_o(i))/\sum_{i=0}^{m-1}(t_o(i) - \min(t_o(i))))$. With this new correlation measure, we recalculate the R^*_{ncc} of the original signal and give the result in Fig. 4(e). Note that the standard normal crests and the weak signal of the substrates are both enhanced, but the step-edge response in H location is eliminated.

C. Step 3: Fusion and Verification

The above analysis explained that neither the comb filter nor the improved NCC approach can achieve an accurate identification of substrate fringes. For investigation, the comb filter essentially exerts a global period matching on the stack profile and thus obtain a merit to detect the weak objects, but the filtered signals might be enhanced incorrectly in the broad gap. On contrast, the improved NCC is capable of discriminating many local abnormalities, but it might fail to identify the weak signals. Obviously, the comb filtered signal and the improved NCC signal are complementary to each other. Therefore, the merits of the two approaches can be merged to improve the substrate identification accuracy.

Here, we present a simple merging scheme by utilizing the candidate fringe locations from the comb filtered signal to sift out the real objects in the improved NCC measure. As shown in Fig. 4(f), the comb filtered signal is first divided into different segments around each peak points (labeled with red

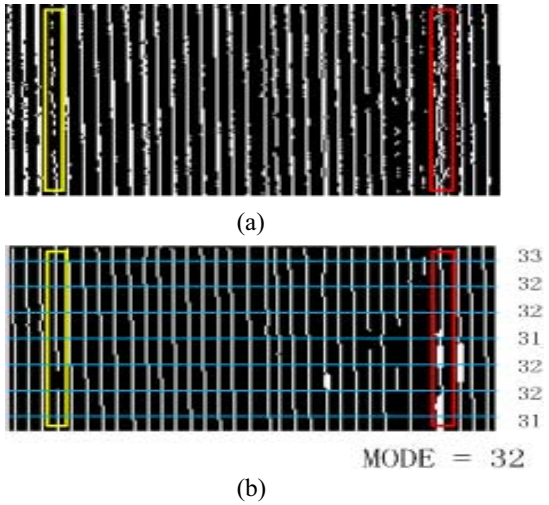

Fig. 8. Ridge line post-processing and counting result. (a) Ridge line obtained from fusion and verification processing. (b) Purified and denoised ridge line and counting result.

circles) with the interval valley points (labeled with green circles) being their boundaries, see the color filled regions. Then, a ZNCC measure is calculated between these peak segments and their counterparts of R^*_{ncc} in Fig. 4(e). Note that only the discrete peak points get the CC values, which are plotted with blue solid circles in Fig. 4(f). In this paper, we use P_{ncc} to indicate the final discrete correlation measure. Because the normal and weak substrate fringes usually have a similar profile shape in both the comb filter and R^*_{ncc} results, they tend to obtain a strong P_{ncc} response. Conversely, the original wide-gap region labeled with H gets obviously different profiles in Fig. 4(c) and (e), and thus resulted in a negative P_{ncc} value. In this way, the real substrate fringes are, finally, identified by directly thresholding the P_{ncc} response. Essentially, the above fusion procedure adopts a posterior verification mechanism, where the potential objects from the global frequency domain analysis are further verified on basis of their similarity to the local matching result.

As shown in Fig. 3, the 1-D fringe detection algorithm is transversely applied to every row of the stack lateral image. After all the peak points are detected, a binary ridge line image can be generated by mapping them into the original 2-D domain. For comparison, the ridge line images from the intermediate comb filtered F_c, improved NCC R^*_{ncc} and the final P_{ncc} are overlaid to the original image and illustrated in Fig. 7. Note that the ridge lines of P_{ncc} in Fig. 7(d) are greatly improved compared to ridge lines in Fig. 7(b) and (c). For examples, a ridge line is incorrectly formed in the blue circle region of Fig. 7(b) and many segments of the disconnect ridge line are obtained in the yellow circle region of Fig. 7(c). However, for the ridgelines of P_{ncc} in Fig. 7(d), the false ridge line is eliminated (see the blue circle region) and the segments of disconnect ridge line are linked in the yellow circle region.

D. Step 4: Post-Processing and Statistical Counting

Due to the influences of complex factors like foreign fibers, burrs and stains, the obtained ridge lines often appear broken with short-range fractures, or touch each other to form "Y" or "X" type junctions. For example, as shown in Fig. 8(a), the sticky clutters, discontinuous and isolated ridge lines might seriously affect the counting accuracy without further processing. Here, we adopt a morphological scheme to purify the ridge line image. An area opening operation is first applied to remove the small noisy interferences. Then, a directional morphological opening with line structure elements along the substrate stripes is utilized to eliminate the sticky clutters. Finally, the small gap is bridged using a directional closing operation. As marked with the red rectangles in Fig. 8(b), the isolated noise and sticky clutters are clearly suppressed after the purification. On the other hand, the broken line segments are linked together to form a complete ridge line as indicated in the yellow rectangle region.

However, the purified ridge lines are not always expected to obtain a perfect result. The small fractures and residual interferences are inevitably seen even with the post-processing. Instead of pursuing an extremely accurate detection with more advanced algorithms, we introduce a statistical counting approach to accommodate the slight detection error. As shown in Fig. 8(b), the counting results along the blue transverse lines with an equidistant interval are shown at the right side near the line ends. Although the counting results might vary with the transverse rows, a majority of them focus on a fixed value, which can be easily obtained by calculating the mode or median of these row of quantities.

IV. Experiment and Validation

In this section, we will conduct extensive experiments and testing to verify the performance of the system based on our proposed algorithms. Several existing line detection algorithms will be simultaneously implemented for comparison.

The image data were captured from a diversity of substrate samples. The substrate counting software was developed with a hybrid programming of LabView and C++ language using the former for GUI design and the latter for algorithm implementation. The configuration of the industrial computer is 2.7 GHz dual-core CPU and 4 GB RAM, and the execution time (including image acquiring time) is about 200 ms for the whole counting algorithm.

A. Qualitative Evaluation and Comparison

The qualitative evaluation is done in two aspects: 1) the challenging data with typical abnormalities are used to verify the capability in a comparative way and 2) a diversity of samples is used to test the adaptability. Here, we only qualitatively evaluate the performance with some representative data.

The classical Canny edge detector [24] and the line segment detector (LSD) [25] method are used for comparison. Both the algorithms make use of the gradient amplitude and direction to detect the linear structures from the stack image, potentially merging some prior shape assumption and constraint. Because the substrate stripes usually have two boundaries, a dual edges suppression mechanism like [19] was adopted to guarantee a single response to each substrate. Because the substrate edge

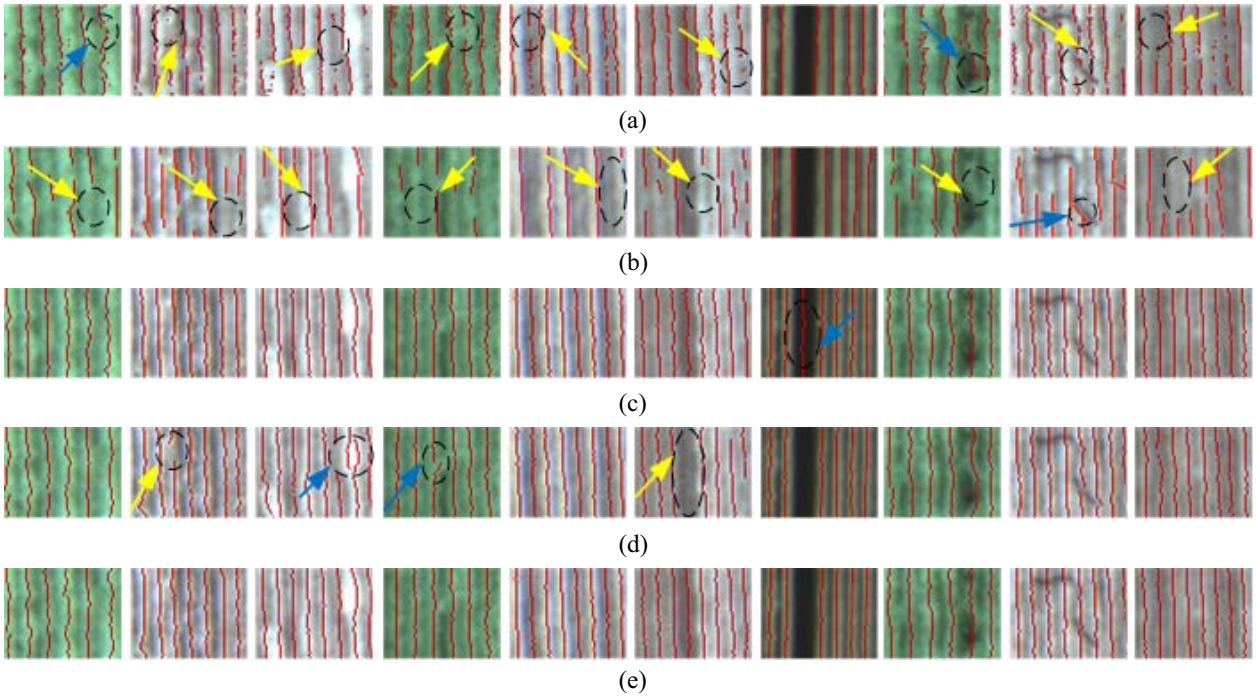

Fig. 9. Comparison of ridge-line images obtained from different methods. The same image patches as shown in Fig. 2(b) are adopted for verification, but the order is rearranged as A–J from left to right. (a) Canny edge detection with a zero lower hysteresis threshold. (b) LSD. (c) Comb filter F_c. (d) Improved NCC R^*_{ncc}. (e) Our algorithm.

often appears very weak, we set the lower hysteresis threshold to zero during the Canny detection.

In Fig. 9, we first choose several typical abnormal images corresponding to the A–J patches in Fig. 2 for evaluation. The line detection results from the single-side Canny operator, LSD method, the comb filtered signal F_c, the improved NCC R^*_{ncc} and our final peak correlation measures P_{ncc} are overlaid on the original images and arranged from top to bottom. Here, the Canny and LSD detectors actually locate the single-side step edges of the substrates, whereas the rest algorithms detect the ridge lines. As observed, both the modified Canny operator and LSD method suffer much from the missed detection (see the yellow arrows) on weak substrate stripes, which is especially serious with the latter. The false line responses (labeled with blue arrows) are also frequently seen in Fig. 9(a) due to the low zero hysteresis threshold used for edge linking, which was particularly set to improve the completeness of detection. Comparatively, the false detection appears rarely in the LSD result except a few cases like the foreign contamination (I). In Fig. 9(c) and (d), the intermediate results of F_c and R^*_{ncc} are simultaneously given to verify the merging effect of our proposed algorithm. Obviously, the final ridge line detection has integrated the merits of F_c and R^*_{ncc}, and thus outperforms the Canny and LSD methods with little false response and missed detection. Therefore, even with the challenging abnormality data, our presented algorithm can still achieve a robust and accurate measurement.

To verify that our algorithm can satisfy the requirement of various kinds of substrates measurement, a diversity of samples with different material, color and surface properties are used for testing. As shown in Fig. 10, a series of stacked substrates including black cigarette box, clothes tag, printed circuit board, plastic bag, and printer paper is arranged sequentially at the top row, and their zoomed stack side images are given at the second row. It can be seen that these stacked substrates obviously vary in geometric and photogrammetric parameters such as stripe width, interstripe gap, substrate color, brightness, and contrast. Without further preprocessing, our proposed algorithm was directly applied to these stack images using the same fixed parameters. As observed from the overlaid ridge line maps at the bottom row, all the substrate stripes are correctly and completely identified in Fig. 10(a)–(d). An exception is with the printed paper stack, where the indistinguishable interval between neighboring substrates makes it difficult to recognize the stripes. This is reflected by the broken or incomplete ridge lines in Fig. 10(e). However, the missed detection of stripes only rarely happened in local regions, which hardly affects the final counting output due to the statistical mode measurement.

B. Quantitative Evaluation

As shown in Fig. 10, ten types of substrates with different material, thickness, color and surface attribute are selected as samples for quantitative evaluation. Their materials include paper, plastic, metal, PCB and so on, and their thickness varies from 0.05 mm to 0.5 mm. In the experiment, every 500 sheets of substrates with the same material are piled in a stack, and 20 stacks with each type are used to capture their side stack images with the developed apparatus.

Because it is difficult to discriminate between the missing detection and the false detection by directly comparing the

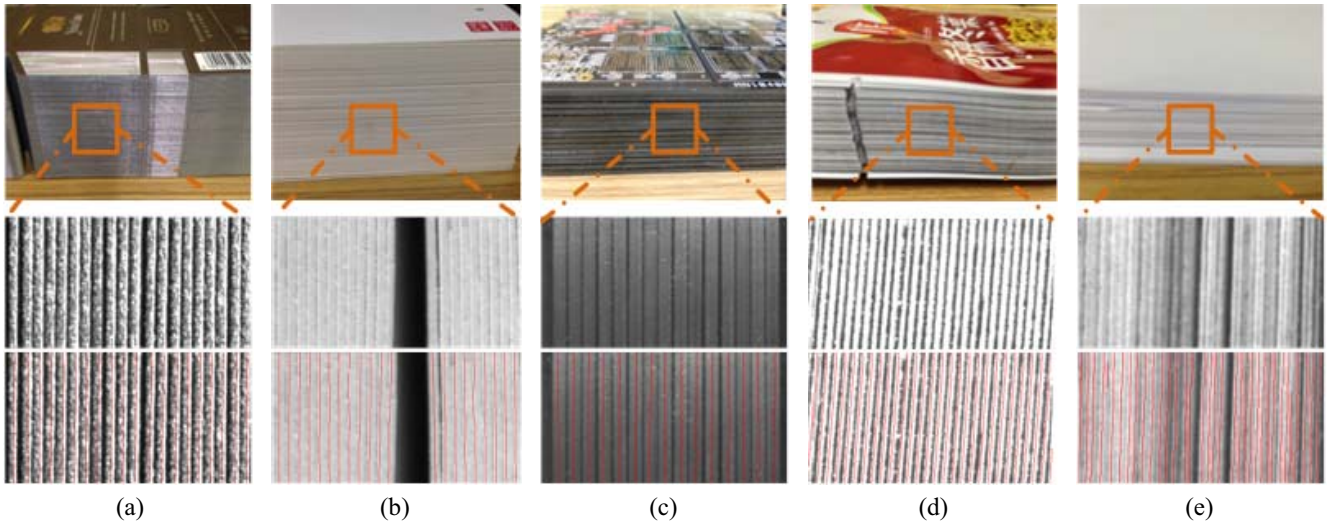

Fig. 10. Demonstration of diverse applicability. The top row is a series of stacked substrates: (a) black cigarette box, (b) clothes tag, (c) printed circuit board, (d) plastic bag, and (d) printer paper. The second row is the zoomed stack side images. The third row is the detected ridge line overlaying on the original image in red.

TABLE I
QUANTITATIVE EVALUATION

Proposed Method			Modified LSD			Modified Canny		
$P_r(\%)$	R_c (%)	$E(\%)$	$P_r(\%)$	$R_c(\%)$	$E(\%)$	$P_r(\%)$	$R_c(\%)$	$E(\%)$
100	99.99	≈ 0.01	99.98	99.63	0.38	99.93	99.86	0.21

apparatus output and the manual counting result, an indirect approach is to use the obtained ridge line image for validation instead. To construct a reference data set for evaluation, a subimage including a fixed number (100 sheets) of substrates is randomly selected from each stack image and the ridge-lines of the substrates are manually delineated, resulting in 200 patches in total.

To compare the ridge-lines from computational algorithms with the manually defined reference, we directly overlap the two binary images and a distance tolerance $D_{\max}$ is adopted to determine their consistency. The pixel of detected substrate stripes is determined as true positive (TP_1) if its distance to the closest reference is less than $D_{\max}$. Otherwise, it is classified into false positive (FP). Similarly, the pixels of ridge-line references can also be divided into true positive (TP_2) and false negative (FN) depending on their distance to the detected stripes. With a similar definition of quantitative indexes to [26], Precision and Recall are defined as $TP_1/(TP_1 + FP)$ and $TP_2/(TP_2 + FN)$, respectively. Precision measures exactness or quality over the detection result, whereas Recall measures completeness or quantity over the reference. To measure the deviation over the detection result, Error is defined as $(FN + FP)/(TP_2 + FN + FP)$. In this application, true negative (TN) has no clear definition and it is deliberately omitted.

We compare the proposed method with the modified LSD and Canny methods on quantitative indexes. Different from the proposed method, these two methods generate edge-line images. Therefore, the ridge-line comparing procedure used in the above evaluation is replaced with edge-line comparing to calculate the quantitative indexes of them. The quantitative indexes of different methods are summarized in Table I. The values of Precision and Recall indexes indicate that the proposed method gets less missing and false detections than other two methods. Furthermore, the maximal error of our method is less than 0.01 % in our experiments. These evaluating results demonstrate the proposed method is quite robust to noise and abnormal circumstances.

V. DISCUSSION AND CONCLUSION

In this paper, we presented a machine vision system for stacked substrates counting on basis of a novel stripe detection algorithm. The robustness of substrate detection was improved by merging a modified correlation measurement and some prior constraints, which include the periodical repetition across the piling profile and the curvilinear shape along the substrates. Our main contribution is to design a framework to combine the merits of global frequency spectrum analysis and local template matching. To accommodate the complex abnormalities in real images, we also heuristically improve the correlation measurement by considering both the original gray-value distribution and the peak similarity. Moreover, a morphological purification and a statistical counting method are further adopted to refine the final output from the generated ridge-line images.

Using a diversity of stacked substrates especially with challenging data and different media, the validation experiments were conducted in a comparative way. It was verified that the proposed algorithm outperforms the conventional Canny edge detector and LSD-based algorithms in both measurement accuracy and robustness to deformations. This was verified not only from the illustration of qualitative experiments but also with

the quantitative indexes (Precision, Recall, and Error). Our method yielded higher Precision and Recall indexes, and lower error value compared to the modified Canny edge operator and LSD method.

However, the performance of our method might appear quite limited in situations like seriously adhering substrates, rough surface, transparent, and low reflection media, as the substrate stripes will become unrecognizable with low contrast, weak edge, and complex interference. To cope with these extremely challenging problems, we will introduce some adaptive imaging technologies to improve the imaging quality, and adopt a machine learning scheme for adhering and incomplete objects detection in our future work.

REFERENCES

[1] B. Bittar and D. Perdoux, "Device for counting products stacked side-by-side," U.S. Patent 5 686 729, Nov. 11, 1997.

[2] D. Petker *et al.*, "Real-time wavelet-based inline banknote-in-bundle counting for cut-and-bundle machines," in *Proc. IS T/SPIE Electron. Imag.*, San Francisco, CA, USA, 2011, Art. no. 787703.

[3] C. Suppitaksakul and M. Rattakorn, "Machine vision system for counting the number of corrugated cardboard," in *Proc. Int. Elect. Eng. Congr. (IEECON)*, 2014, pp. 1–4.

[4] J. L. Mato, M. A. Souto, R. Besteiro, and J. A. Moledo, "Automated counting of palletized slate slabs based on machine vision," in *Proc. 39th Annu. Conf. IEEE Ind. Electron. Soc. (IECON)*, Vienna, Austria, 2013, pp. 2378–2383.

[5] Q. Zhang, B.-Q. Li, Z.-Q. Sun, Y.-J. Li, and C.-Y. Pan, "Solar wafers counting based on image texture feature," in *Proc. Chin. Conf. Image Graph. Technol.*, 2015, pp. 133–141.

[6] P.-H. Wu and C.-H. Kuo, "A counting algorithm and application of image-based printed circuit boards," *J. Appl. Sci. Eng.*, vol. 12, no. 4, pp. 471–479, 2009.

[7] W. Mohan and S. Willits, "Pitch matching detecting and counting system," U.S. Patent 3 790 759, Feb. 5, 1974.

[8] A. Machida and M. Yamai, "Image-based edge detection of stacked sheet media," U.S. Patent 7 490 828, Feb. 17, 2009.

[9] D. Sauer and H. Karl, "Counting disk of sheet counter," CA Patent 7 490 828, Oct. 10, 2006.

[10] Ç. Aytekin, Y. Rezaeitabar, S. Dogru, and I. Ulusoy, "Railway fastener inspection by real-time machine vision," *IEEE Trans. Syst., Man, Cybern., Syst.*, vol. 45, no. 7, pp. 1101–1107, Jul. 2015.

[11] K. Chen and Z. Zhang, "Pedestrian counting with back-propagated information and target drift remedy," *IEEE Trans. Syst., Man, Cybern., Syst.*, vol. 47, no. 4, pp. 639–647, Apr. 2017.

[12] D. Mery *et al.*, "Modern computer vision techniques for X-ray testing in baggage inspection," *IEEE Trans. Syst., Man, Cybern., Syst.*, vol. 47, no. 4, pp. 682–692, Apr. 2017.

[13] J. Rutti, "Method and system for counting stacked items," U.S. Patent 13 206 931, Aug. 10, 2011.

[14] R. Young, R. Reed, and F. Crosdale, "Apparatus and method for counting sheets," European Patent EP 0 743 616 A2, 1996.

[15] D. Petker *et al.*, "Method and system for touchless counting of stacked substrates, especially bundled banknotes," U.S. Patent 9 042 632, May 26, 2015.

[16] E. Auboussier, B. Berthe, and T. Fumey, "Device for counting stacked products," U.S. Patent 7 045 765, May 16, 2006.

[17] R. Harba, B. Berthe, D. Perdoux, and B. Tourne, "Card-counting device," U.S. Patent 12 597 678, Apr. 23, 2008.

[18] T. Chen, Y. Wang, and C. Xiao, "An apparatus and method for real-time stacked sheets counting with line-scan cameras," *IEEE Trans. Instrum. Meas.*, vol. 64, no. 7, pp. 1876–1884, Jul. 2015.

[19] Z. Gang, Y. Shuo, and C. Xiao, "A fast straight-line growing algorithm for sheet-counting with stacked-paper images," in *Proc. Chin. Conf. Pattern Recognit.*, 2014, pp. 418–425.

[20] H. Golnabi and A. Asadpour, "Design and application of industrial machine vision systems," *Robot. Comput.-Integr. Manuf.*, vol. 23, no. 6, pp. 630–637, 2007.

[21] P. Corke, *Robotics, Vision and Control: Fundamental Algorithms in MATLAB*, vol. 73. Cham, Switzerland: Springer, 2011.

[22] I. K. Jung and S. Lacroix, "A robust interest points matching algorithm," in *Proc. 8th IEEE Int. Conf. Comput. Vis. (ICCV)*, vol. 2. Vancouver, BC, Canada, 2001, pp. 538–543.

[23] T. M. Koller, G. Gerig, G. Szekely, and D. Dettwiler, "Multiscale detection of curvilinear structures in 2-D and 3-D image data," in *Proc. 5th IEEE Int. Conf. Comput. Vis.*, Cambridge, MA, USA, 1995, pp. 864–869.

[24] J. Canny, "A computational approach to edge detection," *IEEE Trans. Pattern Anal. Mach. Intell.*, vol. PAMI-8, no. 6, pp. 679–698, Nov. 1986.

[25] R. Grompone von Gioi, J. Jakubowicz, J.-M. Morel, and G. Randall, "LSD: A fast line segment detector with a false detection control," *IEEE Trans. Pattern Anal. Mach. Intell.*, vol. 32, no. 4, pp. 722–732, Apr. 2010.

[26] C. Xiao *et al.*, "Pulmonary fissure detection in CT images using a derivative of stick filter," *IEEE Trans. Med. Imag.*, vol. 35, no. 6, pp. 1488–1500, Jun. 2016.

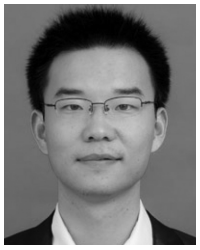

Hong Zhao received the B.Eng. degree in control technology and instrument from the University of South China, Hengyang, China, in 2009 and the M.S. degree in control engineering from Hunan University, Changsha, China, in 2012, where he is currently pursuing the Ph.D. degree.

His current research interests include medical image processing, machine vision, and machine learning.

Rong Dai received the B.Eng. degree in automation from Henan Polytechnic University, Jiaozuo, China, in 2013 and the M.S. degree in control engineering from Hunan University, Changsha, China, in 2017.

His current research interests include machine vision and machine learning.

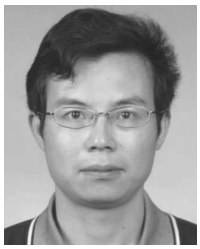

Changyan Xiao received the B.Eng. and M.S. degrees in mechanical and electronic engineering from the National University of Defense Technology, Changsha, China, in 1994 and 1997, respectively, and the Ph.D. degree in biomedical engineering from Shanghai Jiao Tong University, Shanghai, China, in 2005.

He was a Visiting Post-Doctoral Researcher with the Division of Image Processing, Leiden University Medical Center, Leiden, The Netherlands, from 2008 to 2009. Since 2005, he has been an Associate Professor and a Full Professor with the College of Electrical and Information Engineering, Hunan University, Changsha. His current research interests include medical imaging, machine vision, and embedded instrument.